SLAC-PUB-481
September 1968
(ACC)

THE SHIELDING OF MUONS AROUND HIGH ENERGY ELECTRON ACCELERATORS: THEORY AND MEASUREMENT*

W. R. Nelson
Stanford Linear Accelerator Center
Stanford University, Stanford, California

ABSTRACT

The muon flux density and the absorbed dose rate that is produced when a high energy electron beam is completely attenuated in matter is calculated by integrating the muon pair production cross section over the photon distribution in the electromagnetic shower. Several cross section and photon track length formulae are examined. The Fermi-Eyges theory of multiple scattering is applied to the case of 1 to 20 GeV muons penetrating thick shields, and the results are folded into the production theory. An 18 GeV electron beam was used to produce muons in order to verify the theory. The results indicate that the theory, even with multiple scattering included, does not correctly predict the shape of the angular dose rate distribution, although integration over the theoretical and experimental curves gives agreement within experimental error.

(Submitted to Nucl. Instr. and Methods)

*Work supported by the U. S. Atomic Energy Commission.

1. INTRODUCTION

As a result of the calculations by Drell[1] and Ballam[2] during the summer of 1960, it became apparent that a high-energy, high-intensity electron linear accelerator could produce a high-intensity beam of muons by direct electromagnetic pair production. It was also quite evident that one of the most serious shielding problems would arise from the muons produced in a beam stopping device. Now that the Stanford two-mile accelerator is operating at high-energies we would like to present the results of several calculations[3] that we have made and have recently improved on, and we would like to compare these calculations, to an experiment that we have performed using an 18 GeV electron beam.

At both electron and proton machines, high-energy muons are peaked predominately in the forward direction because in both pair production and in nuclear pion production the transverse momenta are of the order of the particle mass (μ = 105.7 MeV). As an example, the characteristic angle for the pair production of 10 GeV muons is 10 milliradians, or about a half of a degree. Consequently, muons are rarely a problem for transversing shielding. On the other hand, they are a problem in the forward direction as a result of their weakly interacting nature – that is, muons with energies less than, say, 50 GeV lose energy essentially by ionization, and hence, a fairly unique range is associated with each energy.

A set of range-energy curves for muons in various materials is provided in Fig. 1. The curves represent an extension of the calculations of Barkas and Berger[4] to energies above 5 GeV, but in addition they include pair production, bremsstrahlung, and nuclear interaction losses of the muon.[5] A similar calculation has been made by Thomas.[6] If one wishes to shield for the complete

range of a 20 GeV muon, it is seen from this figure that it will take about 13 meters of iron.

2. MUON PRODUCTION CALCULATIONS

2.1 Differential Muon Flux Density

The differential muon flux density that is produced when a high energy electron beam is completely attenuated in matter can be calculated by integrating the pair production cross section over the photon distribution in the electromagnetic shower. This can be expressed as

$$\frac{d\Phi}{dE}(E_0, E, \phi) = \frac{2I}{R^2} \int_{E+\mu}^{E_0-m} \frac{d^2\sigma}{d\Omega dE}(k, E, \phi) \frac{d\ell}{dk} dk \; (\mathrm{cm}^{-2} - \mathrm{sec}^{-1} - \mathrm{GeV}^{-1}) \quad . \qquad (1)$$

In this equation, and in the equations that follow,

ϕ is the production angle in lab coordinates,

R is the distance from the target,

I is the beam current in e^-/sec,

E_0 is the total energy of an electron in the beam,

E is the total muon energy ,

k is the energy of a photon in the shower,

m is the rest mass of the electron,

μ is the rest mass of the muon (105.7 MeV), and

$d\ell/dk$ is the differential photon track length, which is the total path length throughout the shower traversed by photons in the energy increment dk about k. The integration limits have been chosen by kinematics and the factor of two comes from the fact that we want both μ^+ and μ^- .

2.2 Differential Photon Track Length

The differential photon track length formula, derived under Approximation A of shower theory is given by[7]

$$\left.\frac{d\ell}{dk}\right)_A = 0.572 \frac{E_0}{k^2} \quad (\text{r.}\ell./\text{GeV}) \quad . \tag{2}$$

Approximation A neglects collision processes such as ionization and excitation, it neglects the Compton effect, and it uses the asymptotic formulae to describe bremsstrahlung and pair production. A comparison of Eq. (2) with Monte Carlo calculations of the longitudinal shower development in copper by Zerby and Moran[8] for several incident electron energies is made in Fig. 2.[9] The symbols represent the Monte Carlo data divided by the Approximation A track length formula, so that perfect agreement would give unity on this figure. Approximation A will be quite good except at the high energy end where it will overestimate the muon flux density. The two solid curves drawn on this figure have been suggested by Tsai and Whitis[10] and by Clement and Kessler.[11] The Tsai and Whitis track length expression has been used at SLAC in the design of a high energy external muon beam for particle physics research. Since we are interested in the low energy muons as well as the high energy ones, the Tsai and Whitis expression will not apply in our calculations. The Clement and Kessler formula (Eq. (3)), however, agrees quite well with the Monte Carlo results over most of the range.

$$k\left.\frac{d\ell}{dk}\right)_{CK} = \frac{0.964\,u}{-\ell n(1-u^2) + 0.686\,u^2 - 0.5\,u^4} \quad (\text{r.}\ell.) \tag{3}$$

where u = fractional photon energy, k/E_0 .

As pointed out by DeStaebler,[9] Eq. (3) can be approximated by

$$k \frac{d\ell}{dk}\Big)_{CK} \approx \frac{0.572}{u} = k \frac{d\ell}{dk}\Big)_{A} \tag{4}$$

$$\text{for} \quad u^2 \ll 1 \quad (\text{or} \quad k \ll E_0)$$

and

$$k \frac{d\ell}{dk}\Big)_{CK} \approx \frac{27/28}{-\ell n(1-u) - 0.5} \geq k \frac{d\ell}{dk}\Big)_{TW} \tag{5}$$

$$\text{for} \quad u^2 \approx 1 \quad (\text{or} \quad k \approx E_0)$$

where $\frac{d\ell}{dk}\Big)_{TW}$ represents the Tsai and Whitis differential track length formula.

2.3 Muon Pair Production Cross Section

The energy-angle distribution of relativistic muons in the small angle approximation has been derived by Tsai[12] by applying the substitution rule to the Schiff[13] formula for the distribution of bremsstrahlung by an electron scattered in the atomic nucleus. This distribution can be written as the probability per radiation length (in the small angle approximation),

$$\frac{d^2\sigma}{d\Omega\, dE}\Big)_T = \frac{1}{2\pi} \left(\frac{m}{\mu}\right)^2 \frac{E^2 \gamma^2 \eta}{k^3 \ell n(183\, Z^{-1/3})}$$

$$\times \left\{ 16\, \eta\lambda(1-\omega) - (2-\omega)^2 + 2\left[(2-2\omega+\omega^2) - 4\eta\lambda(1-\omega)\right] \ell n\left[2\gamma(\omega-1)/\omega\right] \right\} (\text{r.}\ell.^{-1}\text{-GeV}^{-1}\text{-sr}^{-1}) \tag{6}$$

where

$$\omega = k/E$$

$$\gamma = E/\mu$$

$$\lambda = \gamma^2\phi^2 = \left(\frac{\phi}{\mu/E}\right)^2$$

$$\eta = (1+\lambda)^{-2}$$

and where use has been made of the definition of the radiation length

$$\frac{1}{X_0} = 4\alpha\, Z(Z+1)\, r_0^2 \frac{N}{A} \ln\left(183\, Z^{-1/3}\right) \quad (\mathrm{r.\ell.-cm^2-g^{-1}}) \tag{7}$$

where

α = fine structure constant

r_0 = classical radius of electron

A = atomic weight

N = Avogadro's number

and with $Z(Z+1) \rightarrow Z^2$ for high Z. The characteristic angle, which is defined as μ/E, enters in the terms γ, λ, and η. As is seen from Eq. (6), the Z dependence of the muon flux density is governed by a slowly varying log term in the denominator. The difference between an iron target and a lead target, for example, is at most 12%.

Equation (6) and the Clement and Kessler track length formula (Eq. (3)) are presently being used in the muon shielding calculations at SLAC. Until recently we[3] had used a cross section formula due to Drell[1] and we integrated over the Approximation A photon track length (Eq. (2)). The Drell formula is

$$\left.\frac{d^2\sigma}{d\Omega dE}\right)_D = \frac{1}{2\pi}\left(\frac{m}{\mu}\right)^2 \frac{E^2\gamma^2\eta}{k^3 \ln(183\, Z^{-1/3})} \times \left\{\omega^2 + 2\eta\,(1-\omega)(1+\lambda^2)\right\} 2\ln\gamma \tag{8}$$

In Fig. 3 we have plotted the ratio of the two cross sections as a function of the photon energy, k, and for three muon energies, $E = 1$, 5 and 15 GeV in the forward direction. The asymptotes are due to the fact that the photon energy must be greater than $E + \mu$. As was originally pointed out by Tsai,[12] and is observed in Fig. 3, the Drell formula will overestimate the muon flux density by about a factor of two as compared to the Tsai formula. Using Eqs. (2) and (8), Eq. (1) can be integrated exactly to give

$$\frac{d\Phi}{dE}(E_0, E, \phi) = \frac{1}{2\pi}\left(\frac{m}{\mu}\right)^2 \frac{0.572\, I E_0}{\mu^2 R^2 \ln(183\, Z^{-1/3})} \; 2 \ln\gamma \times \left\{ (1 - v^2) - \frac{1}{3}\left[1 - 4v^3\left(1 - \frac{3}{4}v\right)\right]\eta\,(1 + \lambda^2) \right\} \tag{9}$$

where v = fractional muon energy, E/E_0.

Equation (9) is plotted in Fig. 4 (dashed line) as a function of E/E_0 for an incident electron energy of 20 GeV and for several angles. Also shown (solid line) is the numerical integration of Eq. (1) using the Clement and Kessler track length (Eq. (3)) and the Tsai cross section (Eq. (6)). As anticipated, the former overestimates the flux density by as much as a factor of four. The three points are not experimental points but are taken from the section in the SLAC Users Manual on secondary particle beams,[12] and are in agreement with the present theory (solid line).

The differential flux calculations of Tsai[12] have been experimentally verified for 16 GeV/c electrons producing 5.5, 8.0 and 12.0 GeV/c muons at 0° from a 1.8 radiation length berryllium target.[14] The agreement was quite good and they found no difference in the yields of positive and negative muons.

It should be pointed out that both Eqs. (6) and (8), when integrated over all angles, reduce to the Bethe-Heitler formula.[3, 12]

2.4 Integral Muon Flux Density

The integral muon flux density and the absorbed dose rate are given, respectively, by

$$\Phi\,(E_0, E, \phi) = \int_{E}^{E_0 - m - \mu} \frac{d\Phi}{dE'}\, dE' \quad (\mathrm{cm}^{-2} - \mathrm{sec}^{-1}) \tag{10}$$

and

$$\frac{dD}{dt}\,(E_0, E, \phi) = \int_{E}^{E_0 - m - \mu} f(E')\,\frac{d\Phi}{dE'}\, dE' \quad (\mathrm{rad} - \mathrm{sec}^{-1}) \tag{11}$$

where $\frac{d\Phi}{dE'}$ is given by Eq. (1) and where the upper limit of integration is dictated by particle kinematics. The factor $f(E')$ converts particle fluence to absorbed dose. Generally, f is taken outside the integral as a constant such that $10\ \mu/\mathrm{cm}^2\text{-sec}$ gives 1 mrad/hour (which is calculated by using a constant ionization loss of 1.75 MeV $\mathrm{cm}^2\text{-g}^{-1}$) since the error involved in doing this is small. A slightly more accurate method is to consider f to be a function of energy according to the equation

$$f(E') = 1.6 \times 10^{-8}\,\frac{1}{\rho}\,\frac{dT(E')}{dx}\ . (\mathrm{rad\text{-}cm}^2) \tag{12}$$

where $\frac{1}{\rho}\,\frac{dT}{dx}$ is the unrestricted mass stopping power formula given by Barkas and Berger,[4] in $\mathrm{MeV\text{-}cm}^2\text{-g}^{-1}$.

The integral muon flux density (Eq. (10)) versus the fractional muon energy, E/E_0, is plotted in Figs. 5a-5d for electron energies of $E_0 = 5, 10, 15$

and 20 GeV incident on an iron target that completely absorbs the electromagnetic shower. The Clement and Kessler track length and the Tsai cross section were used with Eqs. (1) and (10) which were numerically integrated on the IBM 360 Model 75 computor at SLAC. The conversion to absorbed dose rate can easily be approximated by dividing the ordinate of Fig. 5 by ten, as indicated above.

3. MULTIPLE SCATTERING OF MUONS IN SHIELDS

The distribution function $F(z, y, \theta)$, which describes the multiple elastic scattering of charged particles as they pass through matter, can be obtained by solving the Fermi diffusion equation[7]

$$\frac{\partial F}{\partial z} = -\theta \frac{\partial F}{\partial y} + \frac{1}{W^2} \frac{\partial^2 F}{\partial \theta^2} \tag{13}$$

where $W = 2p\beta/E_s$

$$E_s = \left(\frac{4\pi}{\alpha}\right)^{1/2} m = 21.2 \text{ MeV}$$

and where y and z are in radiation lengths.

Consider a system of Cartesian coordinates with the origin at the point of incidence and the z-axis along the direction of motion of the incident particles. The other two axis will be the x and y axis, and we will consider the projection of motion of the particles on the (z, y) plane, so that $F(z, y, \theta)\, dy\, d\theta$ will be the number of particles at the thickness z having a lateral displacement (y, dy) and traveling at an angle $(\theta, d\theta)$ with the z axis. Because of symmetry, F also represents the distribution in the (z, x) plane, and the independent nature of the x and y orthogonal directions

implies that $F(z, y, \theta_y) \cdot F(z, x, \theta_x)\, dy\, dx\, d\theta_y\, d\theta_x$ represents the general case in three dimensions.

Equation (13) is derived in Rossi and Greisen[7] under the assumption that θ is small, and is solved for the special case of a parallel and infinitely narrow beam of monoenergetic charge particles traversing some scattering substance with no energy loss.

Eyges[15] has treated the same problem by accounting for the energy loss. He assumes that W^2 is some known function of z and neglects the fact that a particle at z has traveled a somewhat greater distance than z due to deviations caused by scattering – a good approximation for high energy particles.

Eyges obtains the result*

$$F(z, y, \theta) = \frac{1}{4\pi [B(z)]^{1/2}} \exp\left[- \frac{\theta^2 A_2 - 2y\theta A_1 + y^2 A_0}{4B} \right] \tag{14}$$

where

$$B(z) = A_0 A_2 - A_1^2 \tag{15}$$

and

$$A_0(z) = \int_0^z \frac{dz'}{W^2(z')} \tag{16}$$

$$A_1(z) = \int_0^z \frac{(z-z')\, dz'}{W^2(z')} \tag{17}$$

$$A_2(z) = \int_0^z \frac{(z-z')^2\, dz'}{W^2(z')} \tag{18}$$

*Equation(14) of Eyges' does not agree with Eq. (14) above, although his other equations do agree with this paper.

If W^2 is constant, Eq. (14) reduces to the Fermi solution as given by Eq. (1.62) in Rossi and Greisen.[7]

If we integrate $F(z, y, \theta)$ either over y or over θ, we get for the angular and lateral distribution functions, respectively

$$G(z, \theta) = \int_{-\infty}^{\infty} F(z, y, \theta)\, dy$$

$$= \frac{1}{2(\pi A_0)^{1/2}} \exp\left(-\frac{\theta^2}{4A_0}\right) \tag{19}$$

and

$$H(z, y) = \int_{-\infty}^{\infty} F(z, y, \theta)\, d\theta$$

$$= \frac{1}{2(\pi A_2)^{1/2}} \exp\left(-\frac{y^2}{4A_2}\right) \tag{20}$$

The fact that Eqs. (19) and (20) are Gaussian in θ and y is a result of the simplifications introduced in the derivation of Eq. (13).[16]

The mean square projected angle of scattering is easily obtained from Eq. (19) as follows:

$$\langle \theta^2 \rangle = \int_{-\infty}^{\infty} \theta^2\, G(z, \theta)\, d\theta = 2A_0(z) \tag{21}$$

and similarly for the mean square lateral displacement

$$\langle y^2 \rangle = \int_{-\infty}^{\infty} y^2\, H(z, y)\, dy = 2A_2(z) \tag{22}$$

The quantities $\langle\theta^2\rangle$ and $\langle y^2\rangle$ can be calculated from Eqs. (21) and (22) when the functional form of $W^2(z')$ is known and integrable.

Since $W = \frac{2p\beta}{E_s}$, a knowledge of $p\beta$ versus range is needed. Numerical solutions to Eqs. (21) and (22) have been obtained[17] and θ_{rms} and y_{rms} are plotted, respectively, in Figs. 6 and 7 as a function of the distance into the shield for various incident momenta. The calculations were made for Fe and for SiO_2, and each calculation was carried out to a residual range corresponding to a $p\beta$ of 100 MeV/c.

If we neglect energy loss (i.e., $p\beta$ = constant), Eqs. (21) and (22) reduce to

$$\langle\theta^2\rangle = \frac{1}{2}\left(\frac{E_s}{p\beta}\right)^2 z \tag{24}$$

$$\langle y^2\rangle = \frac{1}{6}\left(\frac{E_s}{p\beta}\right)^2 z^3 \tag{25}$$

which correspond to Eqs. (1.67) and (1.68), respectively, in Rossi and Greisen.[7] This special case is compared in Fig. 6 and 7 for $p\beta$ = 20 GeV/c and for SiO_2.

4. MUON DOSE RATE THROUGH A THICK SHIELD

Consider a source of muons and a point detector separated by a thick shield as shown in Fig. 8a. A muon produced at a space angle ϕ will intersect the downstream side of the shield at P, provided that no multiple scattering occurs in the shield.

In reality the particle will multiple scatter to some other point, say P', and the space angle Θ locates a symmetric ring of point detectors. The relative positions of points P, P', and O is shown in Fig. 8b, which is a projection

on the downstream side of the shield looking towards the target T. The problem is to take an incident flux density (or dose rate) distribution in angle ϕ and to fold-in the effect of multiple scattering to obtain the resultant distribution in Θ on the downstream side of the shield.

Let

$\Phi(s)\ s\ ds\ d\delta$ = number of muons in $s\ ds\ d\delta$ at point P coming from the target with no shield present,

$\Phi'(r)\ r\ dr\ d\psi$ = total number of muons in $r\ dr\ d\psi$ coming from the target and multiple scattering to point P',

$H(h)\ h\ dh\ d\epsilon$ = probability of multiple scattering into $h\ dh\ d\epsilon$ at point P' relative to an incident direction given by the line TP.

Then

$$\Phi'(r)\ r\ dr\ d\psi = \int_{\delta=0}^{2\pi}\int_{s=0}^{\infty} \Phi(s)\ s\ ds\ d\delta\ \ H(h)\ h\ dh\ d\epsilon \tag{26}$$

Now from the preceding section (Eq. 20), we have

$$H(h) = \Big[H(z,x)\cdot H(z,y)\Big]\Big|_{z=d} = \frac{1}{4\pi A_2}\ e^{-h^2/4A_2} \tag{27}$$

where we have assumed that the distance PP' is equal to the distance PP'' (which is true for small angles), and where A_2 is a function of the incident muon energy and, hence, is a function of the production angle ϕ. Furthermore,

$$s = R\phi \tag{28}$$

$$r = R\Theta \tag{29}$$

$$h^2 = s^2 + r^2 - 2rs\cos(\delta+\psi) \tag{30}$$

and

$$h\, dh\, d\epsilon = r\, dr\, d\psi \tag{31}$$

so that

$$\Phi'(\Theta) = \int_0^\infty \Phi\ (\phi) C(\phi) I_0 \left[C(\phi)\phi\Theta\right] \times \exp\left[-C(\phi)(\phi^2 + \Theta^2)/2\right] \phi d\phi \tag{32}$$

where

$$C(\phi) = R^2/2A_2(\phi) \tag{33}$$

and where

$$I_0\left[C(\phi)\phi\,\Theta\right] = \frac{1}{\pi}\int_0^\pi \exp\left[C(\phi)\phi\,\Theta\cos\delta\right] d\delta \tag{34}$$

is a modified Bessel function of the first kind. We have taken, with no loss of generality (since we expect symmetry), $\psi = 0$ in the derivation of Eq. (32).

Similarly, the absorbed dose rate on the downstream side of the shield, $\frac{dD'(\Theta)}{dt}$, can be calculated from the dose rate excluding multiple scattering, $\frac{dD(\phi)}{dt}$, by

$$\frac{dD'(\Theta)}{dt} = \int_0^\infty \frac{dD(\phi)}{dt} C(\phi)\ I_0\left[C(\phi)\ \phi\,\Theta\right] \times \exp\left[-C(\phi)\ (\phi^2 + \Theta^2)/2\right] \phi d\phi \tag{35}$$

where one could use, for example, Eq. (11) for $\frac{dD(\phi)}{dt}$.

5. MUON EXPERIMENT

5.1 Description of Experiment

The production of muons from a complete shower-absorbing beam dump was measured on the downstream side of a thick steel shield at the Stanford Linear Accelerator Center. The general layout is given in Fig. 9, which is a

plan view of the shielding that separates the inside of End Station B on the right from the B Target Room on the left. The electron beam enters the B Target Room from left to right and is normally steered into the beam dump at the top or the beam dump at the bottom of the center-line labeled "positron beam port." Frequently, a positron beam is brought out the center port into the end station. For our experiment, however, an 18 GeV electron beam was directed into the lower beam dump, which consisted of 15 radiation lengths or more of water-cooled copper plates. A detector plate was well centered along the electron beam direction on the downstream side of the iron shielding. The shield was 4.27 meters thick, and all openings were plugged in order to reduce the background radiation. For a detector we used LiF (Harshaw TLD-700)* which was 99.993% enriched in Li^7 and hence did not significantly respond to neutrons. LiF is a thermoluminescent material that can be used to measure energy deposition over a wide dose range with a flat energy response and good precision, and its usefulness for absorbed dose measurements around high energy accelerators has been previously demonstrated.[18, 19, 20]

The LiF powder was poured into polyethylene tubing having an inner diameter of 0.584 mm and an outer diameter of 0.965 mm. By vibrating the powder we achieved a bulk density of 1.6 g/cm^3 and a fairly good uniformity. The tubing was placed in concentric circular grooves that were precisely milled in a 6.35 mm lucite plate. The radii covered a range of angles from essentially 0° to 3.2^o, as measured from the dump located 5.19 meters upstream in the Target Room. In addition, an ionization chamber was aligned on the 0° direction just downstream of the detector plate.

The 18 GeV electron beam was brought into the Target Room at about 600 Watts for approximately 5 minutes in order to steer the beam on the center

*Harshaw Chemical Company, Cleveland, Ohio.

of a ZnS screen that had been precision-aligned on the face of the dump. The beam power was then increased to 16.2 kW and held there for 258 minutes during which time the beam was extremely steady in both position and magnitude.

5.2 Results and Comparison with Theory

After the exposure, the detector plate was removed and the LiF was subsequently read-out, the results of which are plotted in Fig. 10. In the upper left is a view of the detector plate, looking towards the beam. The plate was marked off into octants and the LiF powder in each segment was vibrated out of the polyethylene tubing into a weighing pan. After weighing, the powder was heated and read-out in a commercial TLD reader,* a background was subtracted, and the resultant light output was converted to absorbed dose in rad.

The LiF powder was calibrated in terms of absorbed dose using a Victoreen R-Meter** and a Cs^{137} source and the calibration exposure was done under charged particle equilibrium conditions.[21] Corrections were made for temperature, pressure, and the NBS calibration of the R meter.

In Fig. 10 the experimental results are compared with the theory (solid line) using the Tsai cross section and the Clement and Kessler track length (neglecting multiple scattering). There were 4.27 meters of steel shielding between the source and the detector, which meant that only those muons having energies greater than 6 GeV were able to get through. As a result, the absorbed dose rate integration was taken from 6 GeV to (18-m-μ) GeV, and the conversion factor f was evaluated within the integral at energies equal to (E-6) GeV. The maximum error of $\pm$ 10% on the theoretical curve is the

*Isotopes, Inc. (ConRad), Westwood, New Jersey.
**Victoreen Instrument Co., Cleveland, Ohio.

combined effect of the uncertainty in the source-to-detector distance, the uncertainty in the beam power, and the uncertainty in the total integration time.

The TLD data is shown along with the one point at 0° which represents the rad dose in air that was integrated by the ion chamber (a cylinder having a radius of 1 inch and length of 5 inches). At most the ion chamber could have subtended an angle of 10 milliradians, which is within the relatively flat dose rate region measured by the LiF. The maximum error of each of the LiF data points is about $\pm 10\%$.

The disagreement between the solid line and the data is not surprising in view of the fact that the theory does not include shower divergence and multiple scattering, both of which will cause the distribution to flatten out. If one integrates the experimental and theoretical dose distributions over all angles, the resulting two numbers agree within 20% of each other.

Since the experimental data does not extend past 57 mradians, there is some doubt as to how to extrapolate the experimental curve needed for the integration. What was done was to fit (by eye) the data between 41 and 57 mradians with a straight line. Within this limitation, the theory appears to correctly predict the total integrated muon dose (rad - sq. mradian).

The spreading effect caused by multiple scattering in the shield was calculated by using Eq. (35) with $\frac{dD(\phi)}{dt}$ replaced by the solid line, $D(\phi)$, of Fig. 10. In order to perform the integration, a functional form for $A_2(\phi)$ was needed. This was obtained by calculating the average energy of those muons that are incident upon the shield but still get through, according to

$$\overline{E}(\phi) = \frac{\int_{6}^{18\text{-m-}\mu} E \frac{d\Phi(\phi)}{dE}\, dE}{\int_{6}^{18\text{-m-}\mu} \frac{d\Phi(\phi)}{dE}\, dE} \tag{36}$$

and then by calculating $A_2(\phi)$ from Eq. (18) with $z = d$.

The result of this integration is plotted as the broken line in Fig. 10. It agrees with the experimental results better than the theory without multiple scattering does. However, it appears as if multiple scattering in the shield cannot, by itself, resolve the discrepancy between the theory and the experiment. Possibly the effect of nuclear form factors and/or the fact that the shower divergence has not been included in the theory could provide the answer to the disagreement. It should be pointed out that there appears to be a dip in the data at 0° even though this is within the maximum experimental error ($\pm$ 10%).

In a recent paper, Bathow et al.[22] published the results of a 4 and 6 GeV muon shielding experiment. They compared their measurements with a calculation by Clement and Kessler which included form factors but not multiple scattering. Bathow et al. indicate that they must correct the theory for multiple scattering in the shield in order to obtain agreement with experiment.

6. SUMMARY

The differential and integral muon flux densities and the absorbed dose rate that is produced when a high energy electron beam is completely attenuated in matter has been calculated and has been compared with an experiment at an incident electron energy of 18.0 GeV. The theory correctly predicts the total integrated dose that penetrates a 4.27 meter iron shield, but the shape of the angular distribution is not as broad as indicated by experiment.

Multiple scattering in the shield is reviewed and a calculation is made which folds multiple scattering into the theory, with the expected result that the angular distribution flattens out. However, multiple scattering by itself cannot fully explain the experimental data and it is suggested that the discrepancy might be due to the fact that the theory neglects nuclear form factor effects.

A small contribution conceivably might come from shower divergence, although this is unlikely.

7. ACKNOWLEDGEMENT

The author expresses his appreciation to Dr. H. DeStaebler for suggesting the problem, to Dr. E. Seppi for providing some of his accelerator time in order to perform the experiment, to Mr. T. Ginn for carefully reading the TLD, and to the Health Physics and the Operations groups at SLAC. A special thanks to Dr. G. Svensson for critically reviewing this paper.

REFERENCES

1. S. D. Drell, "Production of particle beams at very high energies," Hansen Laboratory of Physics Report M-200-7A, Stanford University, Stanford, California (August 1960), unpublished; Phys. Rev. Letters 5, 278 (1960); Rev. Mod. Phys. 33, 458 (1961).
2. J. Ballam, "Computation of secondary-particle yields from high-energy electron accelerators," Hansen Laboratory of Physics Report M-200-8, Stanford University, Stanford, California (August 1960), unpublished.
3. W. R. Nelson, "Muon production calculations for muon shielding," SLAC Technical Note TN-66-37, Stanford Linear Accelerator Center, Stanford University, Stanford, California (August 1966), unpublished.
4. W. H. Barkas and M. J. Berger, "Tables of energy losses and ranges of heavy charged particles," National Aeronautics and Space Administration Report NASA-SP-3013 (1964).
5. P. J. Hayman, N. S. Palmer, and A. W. Wolfendale, Proc. Roy. Soc. 275A, 391 (1963).
6. R. H. Thomas, "Energy loss of high energy muons," University of California Lawrence Radiation Laboratory Report UCID-10010, University of California, Berkeley, California (July 1964).
7. B. Rossi and K. Greisen, Rev. Mod. Phys. 13, 240 (1941); B. Rossi, High-Energy Particles (Prentice-Hall, Englewood Cliffs, New Jersey, 1952).
8. C. D. Zerby and H. S. Moran, J. Appl. Phys. 34, 2445 (1963); Oak Ridge National Laboratory Reports ORNL-3329 (1962) and ORNL-TM-422 (1962) (unpublished), Oak Ridge National Laboratory, Oak Ridge, Tennessee. Also, private communication.

9. H. DeStaebler, Stanford Linear Accelerator Center, Stanford University, Stanford, California (private communication).

10. Y. S. Tsai and V. Whitis, Phys. Rev. 149, 1248 (1966).

11. G. Clement and P. Kessler, Nuovo Cimento 37 (3), 876 (1965); G. Clement, Compt. Rend. 257, 2971 (1963).

12. Y. S. Tsai, "Estimates of secondary-beam yields at SLAC," SLAC Users Handbook, D. 3-3, Stanford Linear Accelerator Center, Stanford University, Stanford, California.

13. L. I. Schiff, Phys. Rev. 83, 252 (1951).

14. A. Barna, J. Cox, F. Martin, M. L. Perl, T. H. Tan, W. T. Toner, T. F. Zipf, and E. H. Bellamy, Phys. Rev. Letters 18, 360 (1967).

15. L. Eyges, Phys. Rev. 74, 1534 (1948).

16. W. H. Barkas, Nuclear Research Emulsions, Volume I. Techniques and Theory (Academic Press, New York and London, 1963); p. 291.

17. W. R. Nelson,"Multiple elastic scattering of muons with energy loss," SLAC Technical Note TN-66-41, Stanford Linear Accelerator Center, Stanford, California (September 1966), unpublished.

18. T. M. Jenkins, J. K. Cobb, W. R. Nelson, and R. C. McCall, Nucl. Instr. and Methods 37, 174 (1965).

19. Walter R. Nelson, Theodore M. Jenkins, Richard C. McCall, and Joseph K. Cobb, Phys. Rev. 149, 201 (1966).

20. G. K. Svensson, R. C. McCall, T. M. Jenkins, W. R. Nelson, "Use of thermo-luminescent dosimeters in high energy health physics," Report No. SLAC-PUB-500, Stanford Linear Accelerator Center, Stanford University, Stanford, California (1968).

21. F. H. Attix, W. C. Roesch, and E. Tochilon, Eds., Radiation Dosimetry, Volume I: Fundamentals, Second Edition (Academic Press, New York and London, 1968).

22. G. Bathow, E. Freytag, K. Tesch, Nucl. Instr. and Methods 51, 56 (1967).

LIST OF FIGURES

7. RMS lateral displacement due to multiple elastic scattering of muons of various incident momenta in iron and silicon dioxide.

8. (a) Shielding diagram showing source at T and detector positions at P (unscattered) and P' (scattered).

   (b) Downstream plane of shield with relative positions of points O, P, and P' (looking towards the target).

9. Plan view of experimental set-up.

10. Comparison of differential absorbed dose measurements with theory (using $E_0 = 18.0$ GeV, $E = 6.0$ GeV, $P = 16.2$ kW, $t = 258$ min, and $R = 5.19$ m).

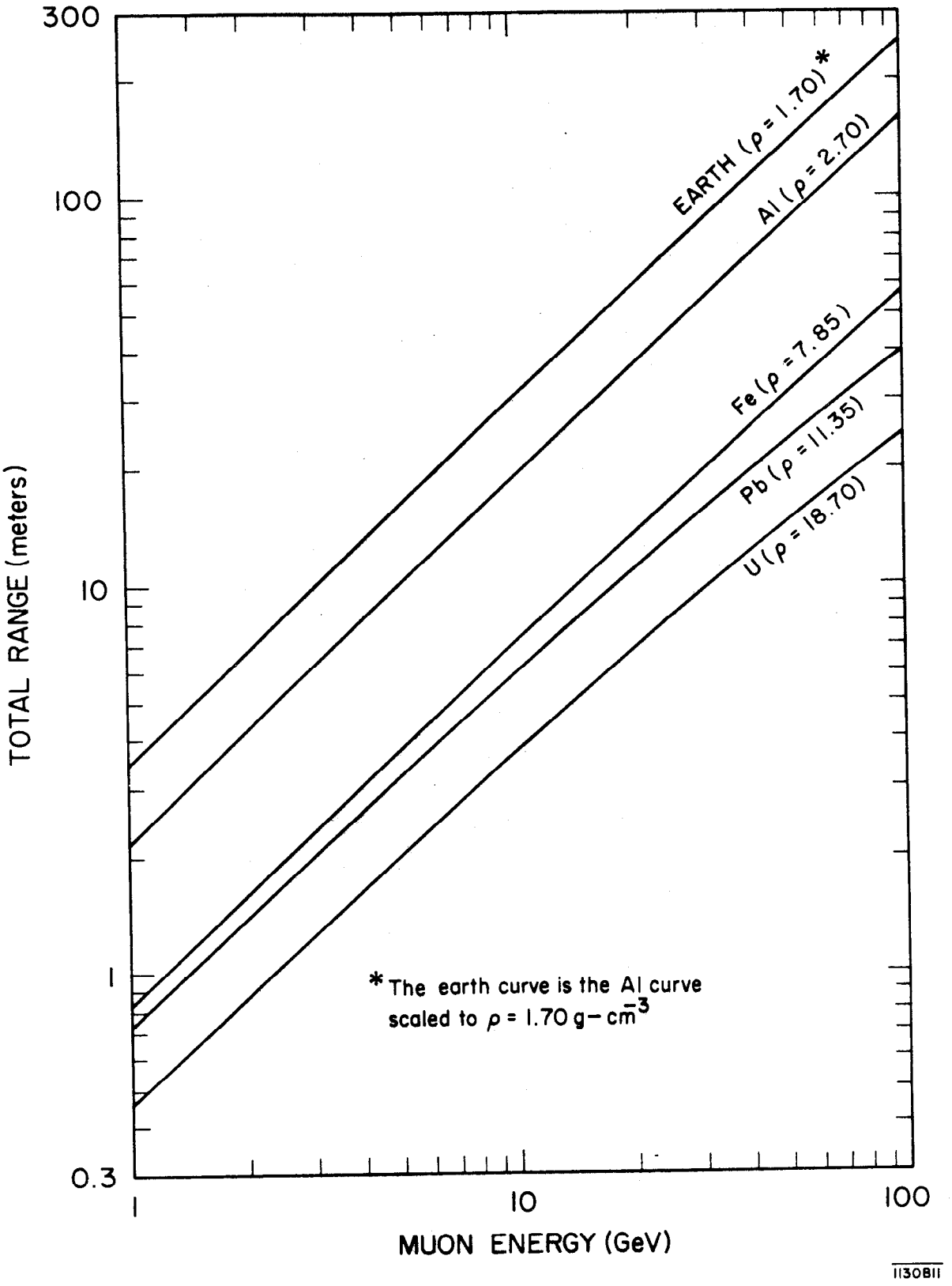
300
100
10
1
0.3
TOTAL RANGE (meters)
1
10
100
MUON ENERGY (GeV)
EARTH (ρ = 1.70)*
Al (ρ = 2.70)
Fe (ρ = 7.85)
Pb (ρ = 11.35)
U (ρ = 18.70)
* The earth curve is the Al curve scaled to ρ = 1.70 g−cm⁻³
1130B11

Fig. 1

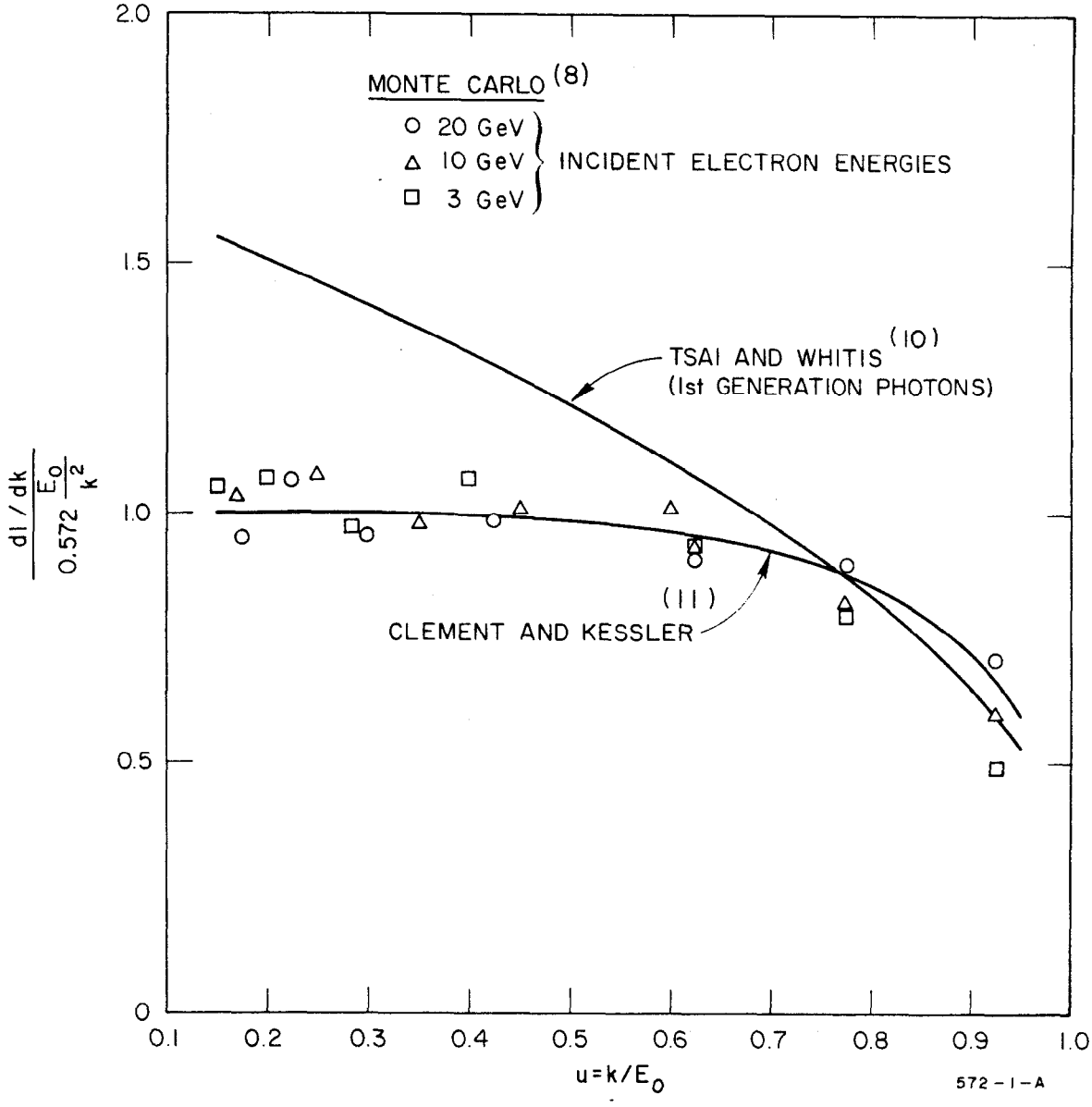
MONTE CARLO (8)
20 GeV
10 GeV
3 GeV
INCIDENT ELECTRON ENERGIES
TSAI AND WHITIS (10)
(1st GENERATION PHOTONS)
(11)
CLEMENT AND KESSLER
$\frac{dI/dk}{0.572 \frac{E_0}{k^2}}$
$u = k/E_0$
572-1-A

Fig. 2

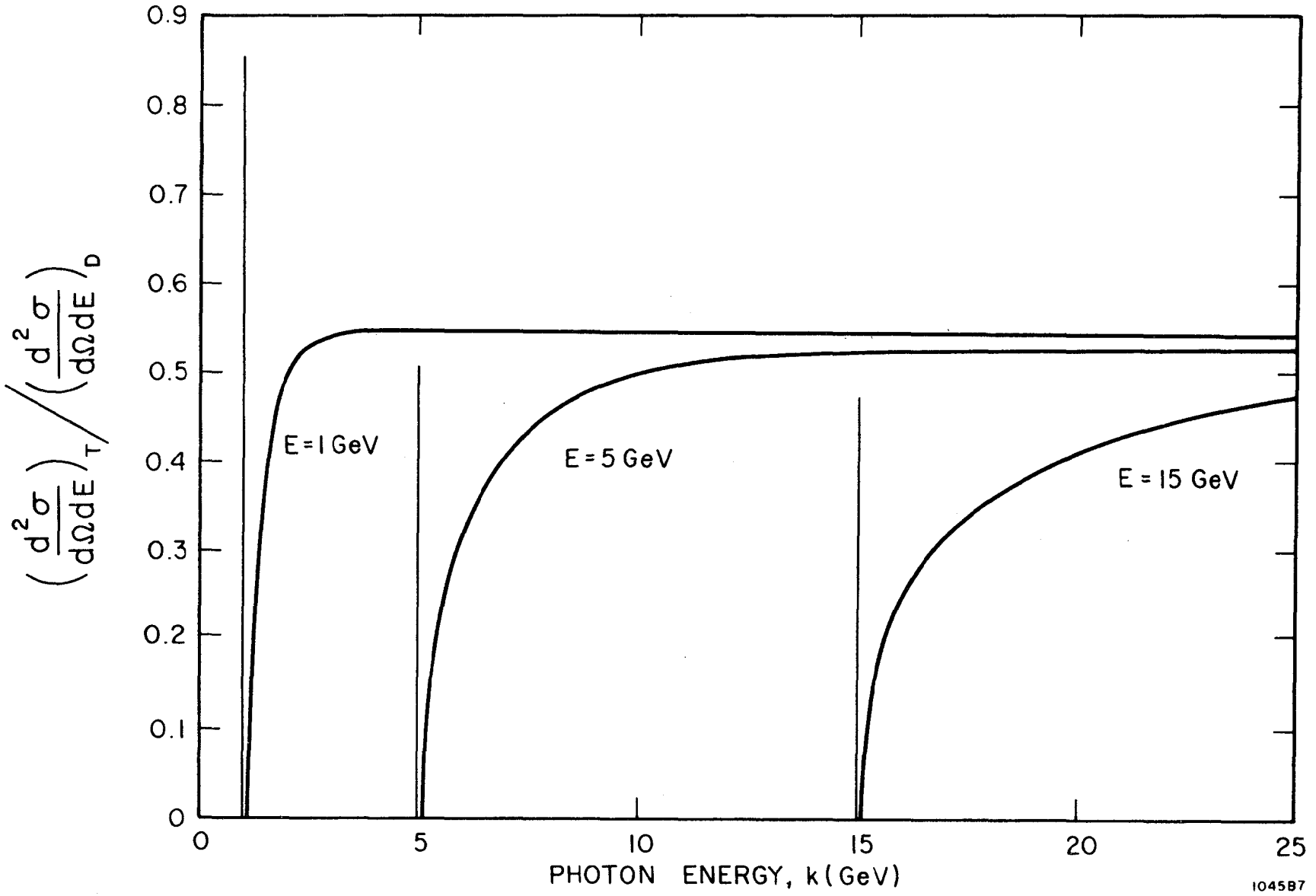
0.9
0.8
0.7
0.6
0.5
0.4
0.3
0.2
0.1
0
$\left(\frac{d^2\sigma}{d\Omega dE}\right)_T \Big/ \left(\frac{d^2\sigma}{d\Omega dE}\right)_D$
E = 1 GeV
E = 5 GeV
E = 15 GeV
0
5
10
15
20
25
PHOTON ENERGY, k (GeV)
1045B7

Fig. 3

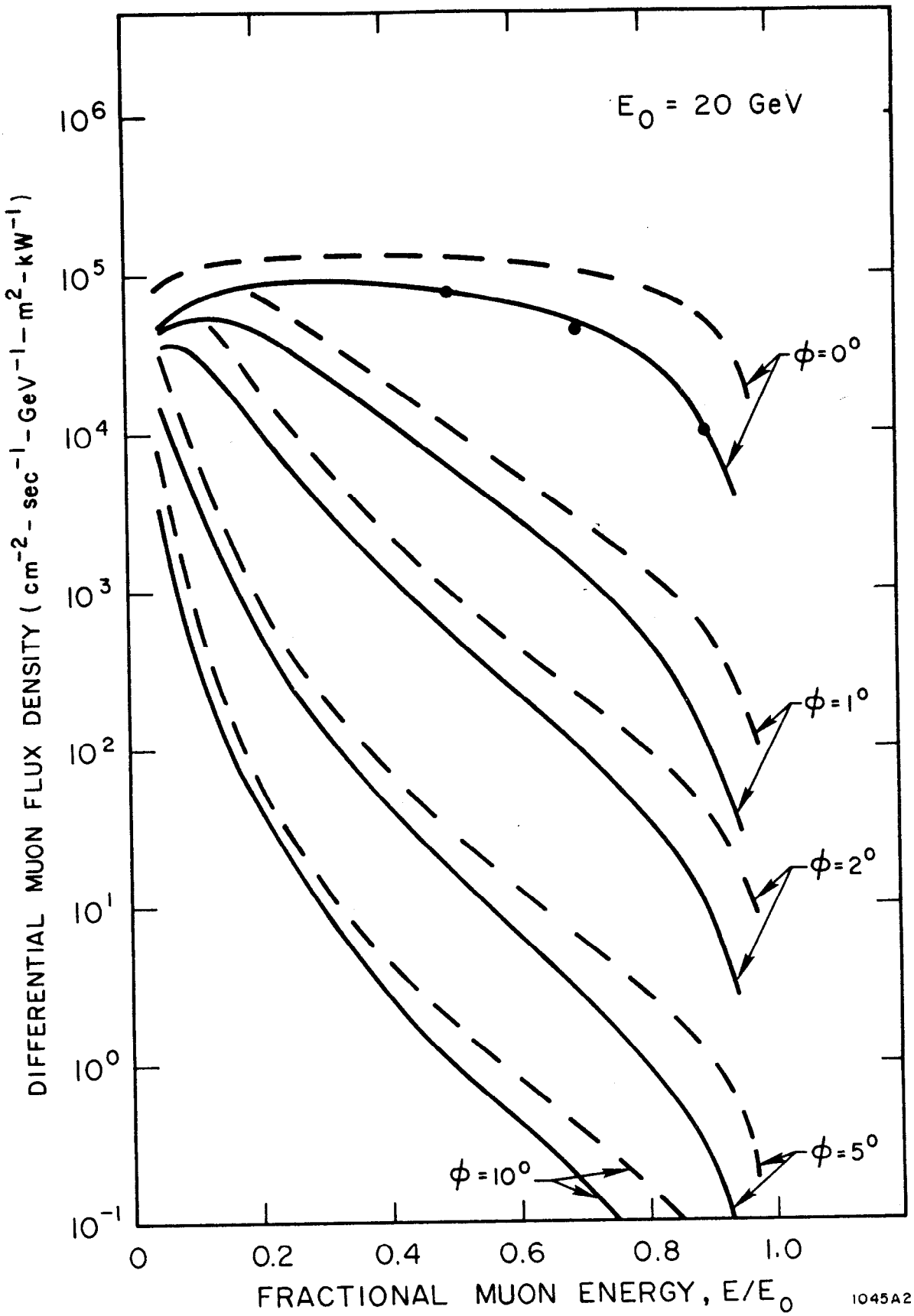
E_0 = 20 GeV
10^6
10^5
10^4
10^3
10^2
10^1
10^0
10^{-1}
DIFFERENTIAL MUON FLUX DENSITY (cm^{-2} - sec^{-1} - GeV^{-1} - m^2 - kW^{-1})
$\phi = 0^\circ$
$\phi = 1^\circ$
$\phi = 2^\circ$
$\phi = 5^\circ$
$\phi = 10^\circ$
0
0.2
0.4
0.6
0.8
1.0
FRACTIONAL MUON ENERGY, E/E_0
1045A2

Fig. 4

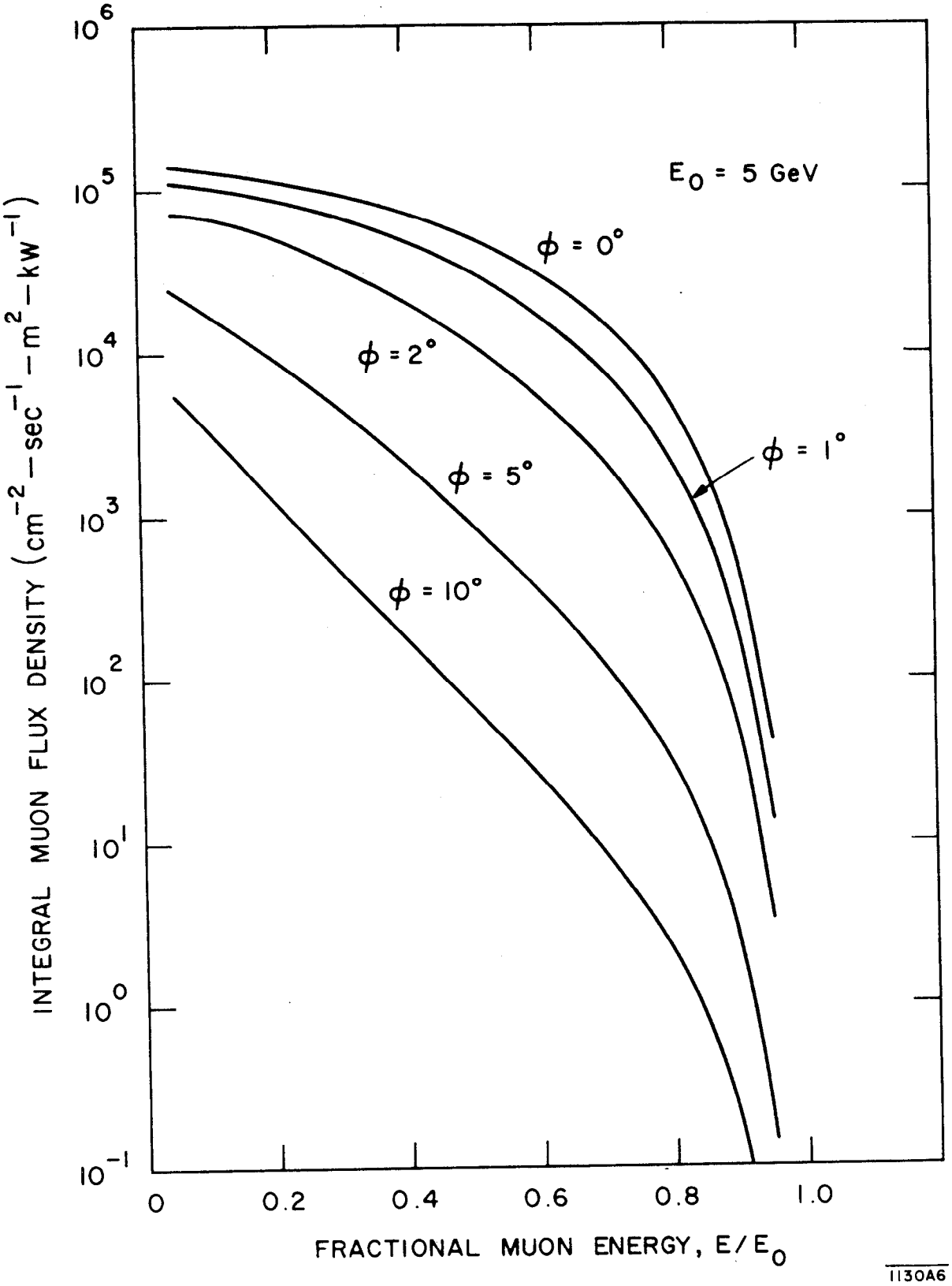
10^6
10^5
10^4
10^3
10^2
10^1
10^0
10^{-1}
INTEGRAL MUON FLUX DENSITY (cm^{-2} — sec^{-1} — m^2 — kW^{-1})
E_0 = 5 GeV
ϕ = 0°
ϕ = 1°
ϕ = 2°
ϕ = 5°
ϕ = 10°
0
0.2
0.4
0.6
0.8
1.0
FRACTIONAL MUON ENERGY, E/E_0
1130A6

Fig. 5a

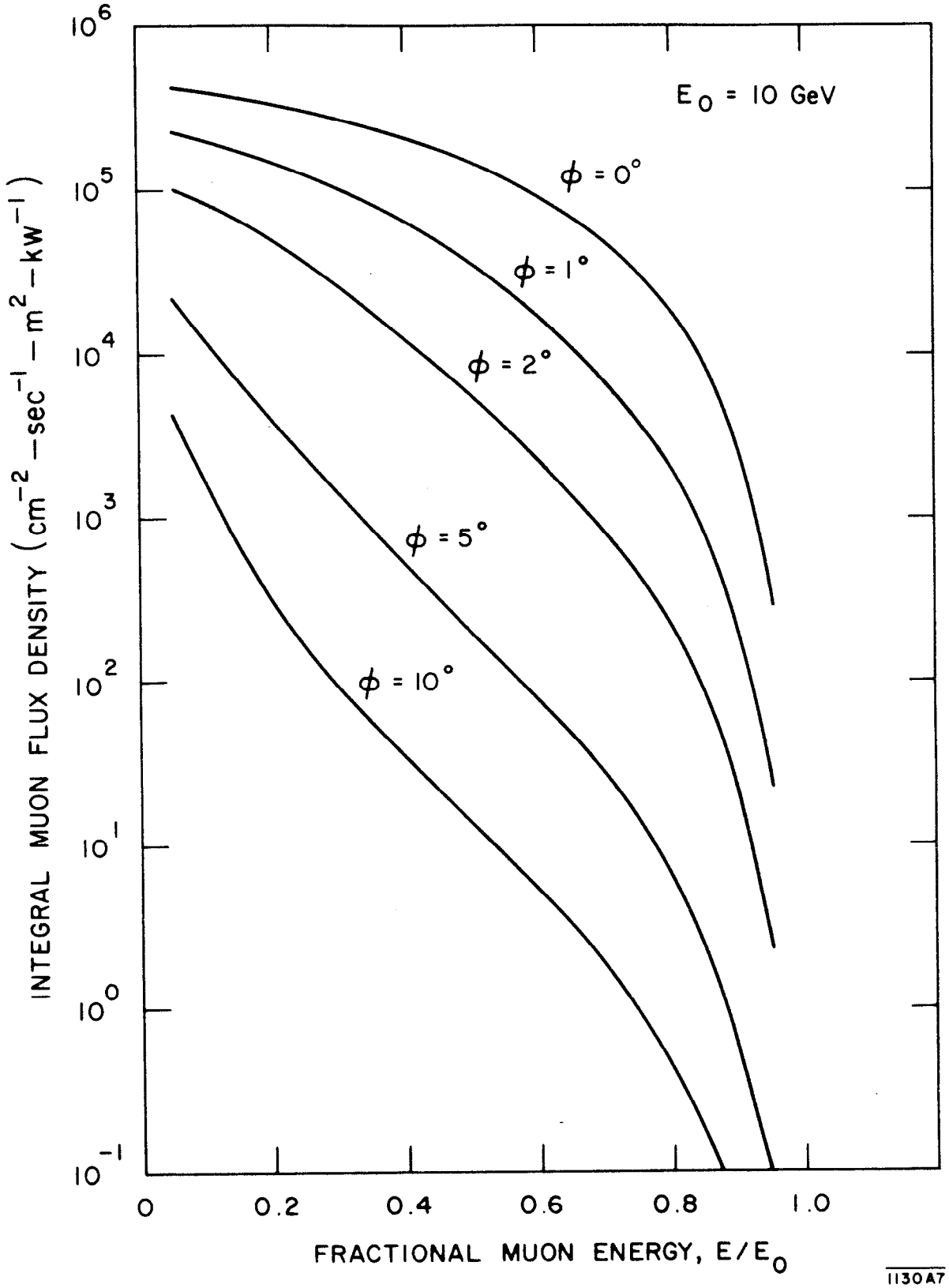
E_0 = 10 GeV
ϕ = 0°
ϕ = 1°
ϕ = 2°
ϕ = 5°
ϕ = 10°
INTEGRAL MUON FLUX DENSITY (cm^{-2}-sec^{-1}-m^{2}-kW^{-1})
10^6
10^5
10^4
10^3
10^2
10^1
10^0
10^{-1}
0
0.2
0.4
0.6
0.8
1.0
FRACTIONAL MUON ENERGY, E/E_0
1130A7

Fig. 5b

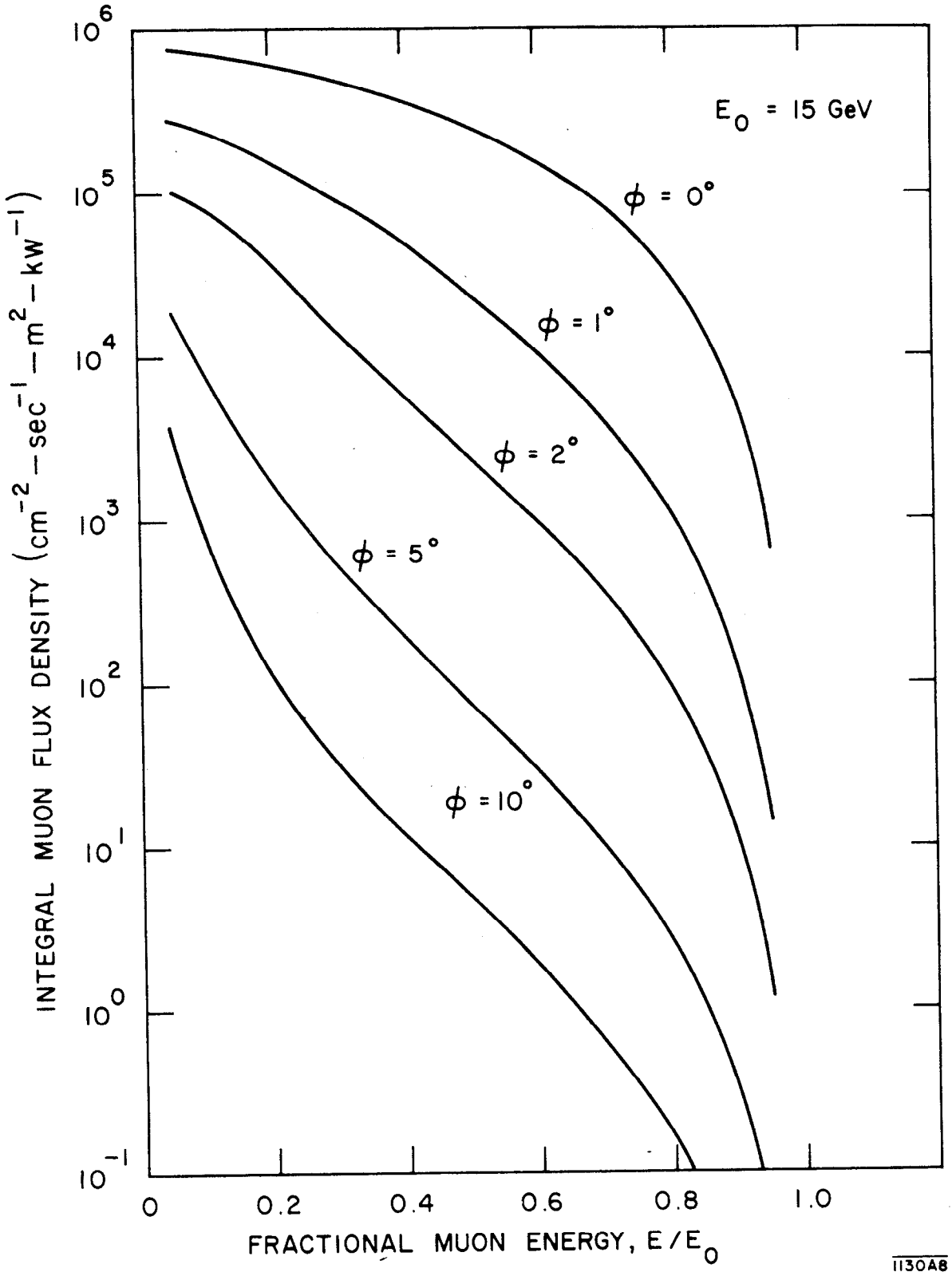
E_0 = 15 GeV
ϕ = 0°
ϕ = 1°
ϕ = 2°
ϕ = 5°
ϕ = 10°
INTEGRAL MUON FLUX DENSITY ($cm^{-2}-sec^{-1}-m^{2}-kW^{-1}$)
10^6
10^5
10^4
10^3
10^2
10^1
10^0
10^{-1}
0
0.2
0.4
0.6
0.8
1.0
FRACTIONAL MUON ENERGY, E/E_0
1130A8

Fig. 5c

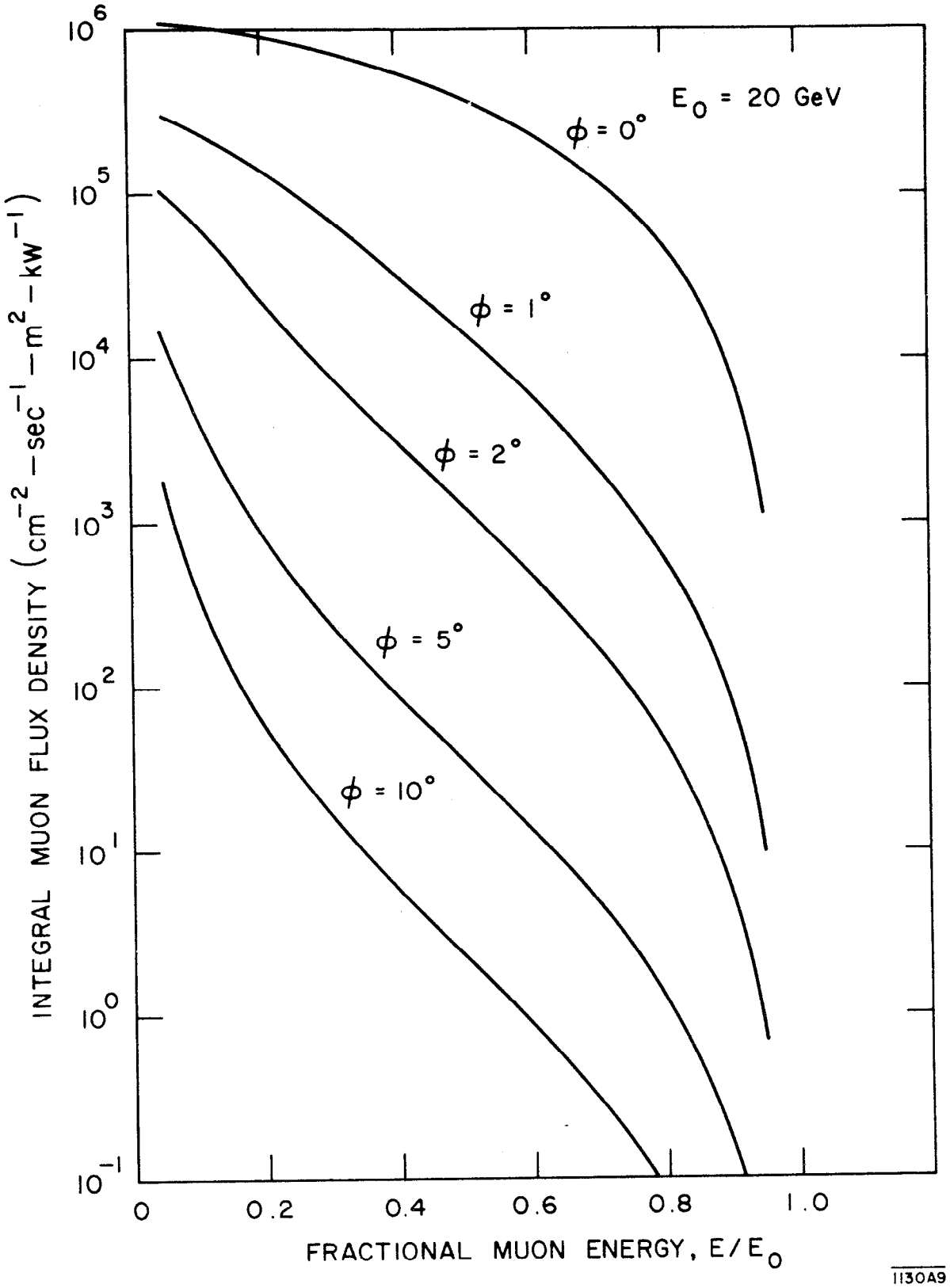
E_0 = 20 GeV
ϕ = 0°
ϕ = 1°
ϕ = 2°
ϕ = 5°
ϕ = 10°
INTEGRAL MUON FLUX DENSITY ($cm^{-2}-sec^{-1}-m^{2}-kW^{-1}$)
10^6
10^5
10^4
10^3
10^2
10^1
10^0
10^{-1}
0
0.2
0.4
0.6
0.8
1.0
FRACTIONAL MUON ENERGY, E/E_0
1130A9

Fig. 5d

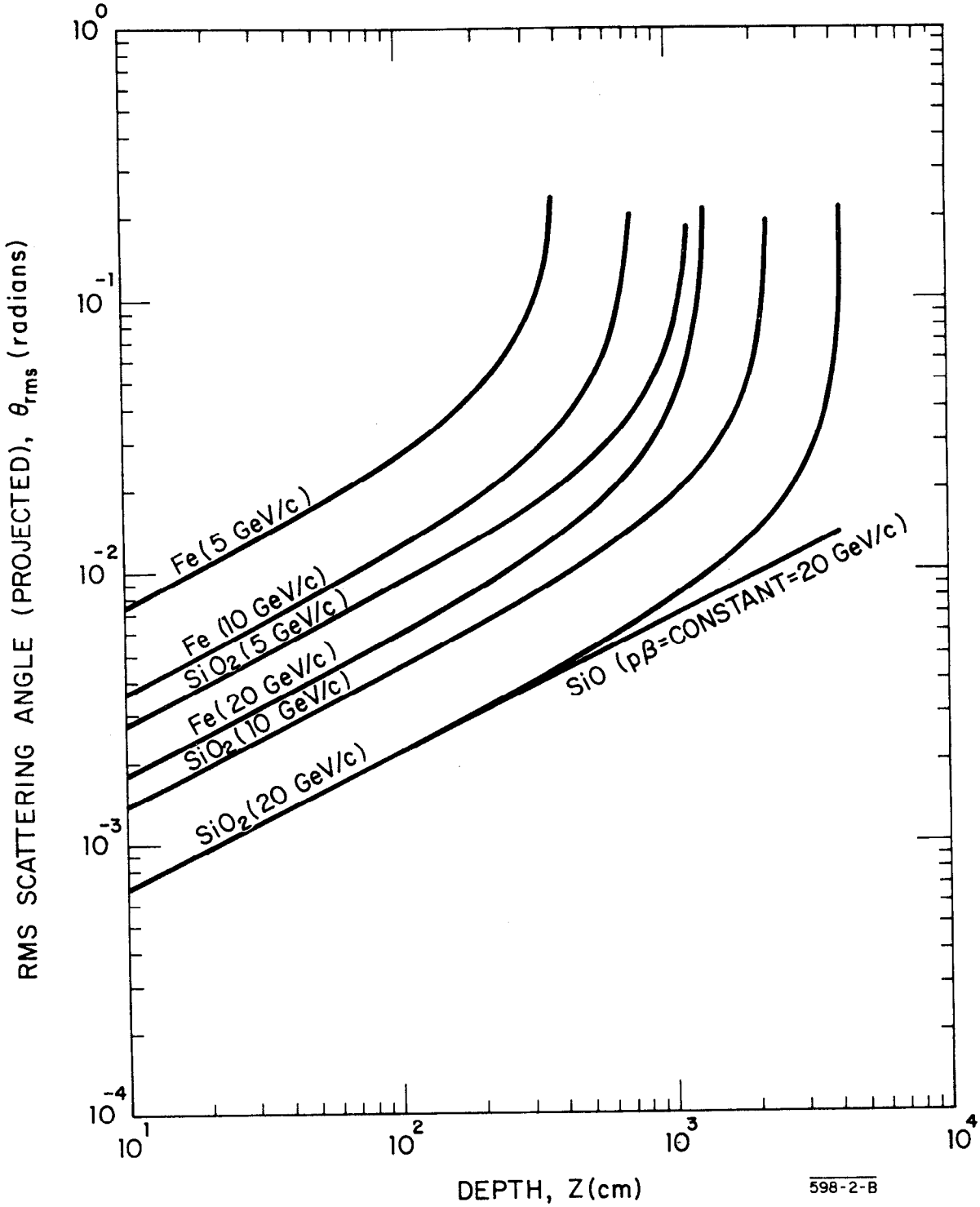
RMS SCATTERING ANGLE (PROJECTED), θ_{rms} (radians)
10^0
10^{-1}
10^{-2}
10^{-3}
10^{-4}
10^1
10^2
10^3
10^4
DEPTH, Z(cm)
Fe(5 GeV/c)
Fe (10 GeV/c)
SiO_2(5 GeV/c)
Fe(20 GeV/c)
SiO_2(10 GeV/c)
SiO_2(20 GeV/c)
SiO (pβ=CONSTANT=20 GeV/c)
598-2-B

Fig. 6

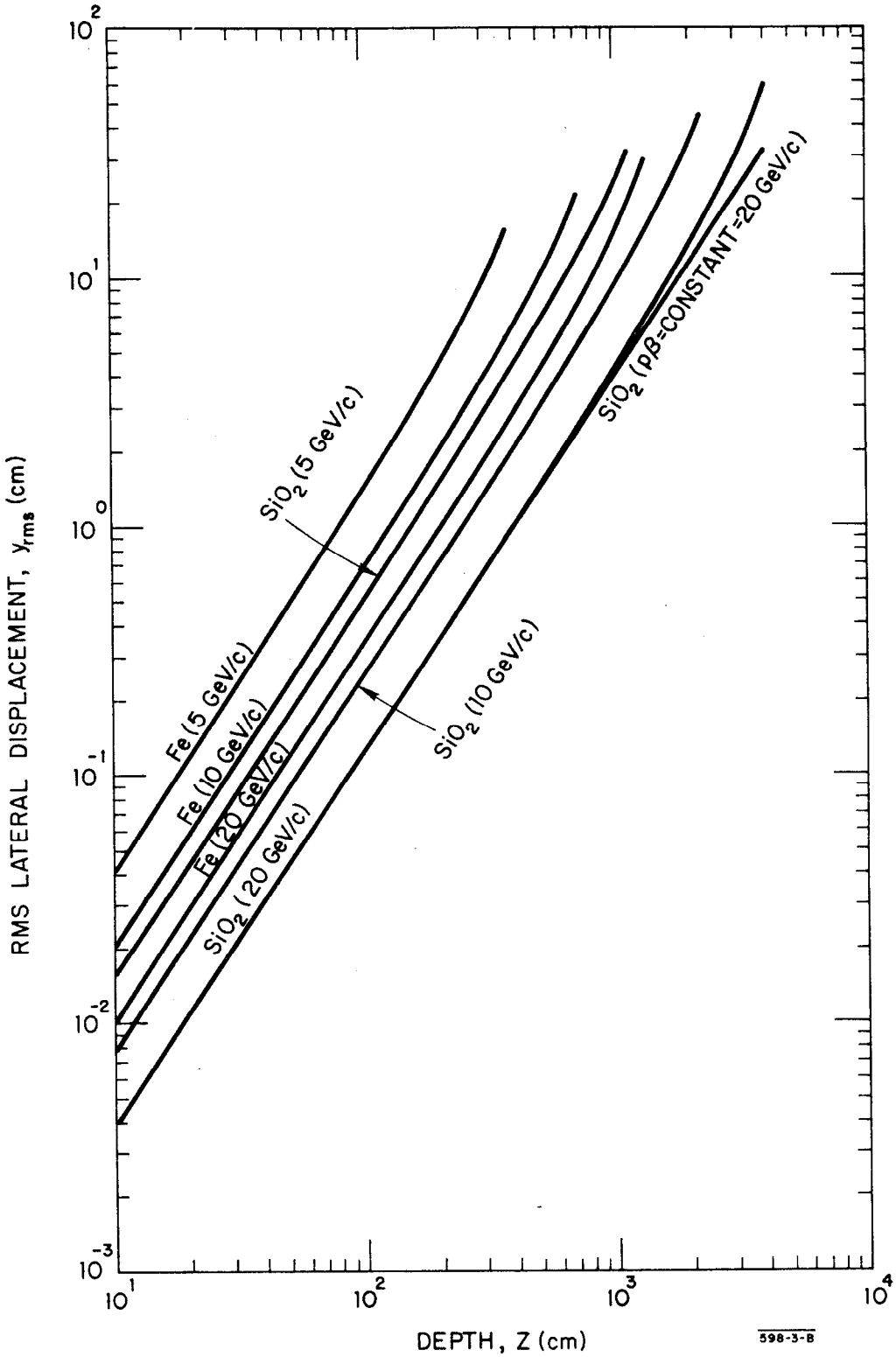
RMS LATERAL DISPLACEMENT, y_{rms} (cm)
DEPTH, Z (cm)
10^2
10^1
10^0
10^{-1}
10^{-2}
10^{-3}
10^1
10^2
10^3
10^4
SiO_2 (5 GeV/c)
SiO_2 ($p\beta$=CONSTANT=20 GeV/c)
Fe (5 GeV/c)
Fe (10 GeV/c)
Fe (20 GeV/c)
SiO_2 (20 GeV/c)
SiO_2 (10 GeV/c)
598-3-8

Fig. 7

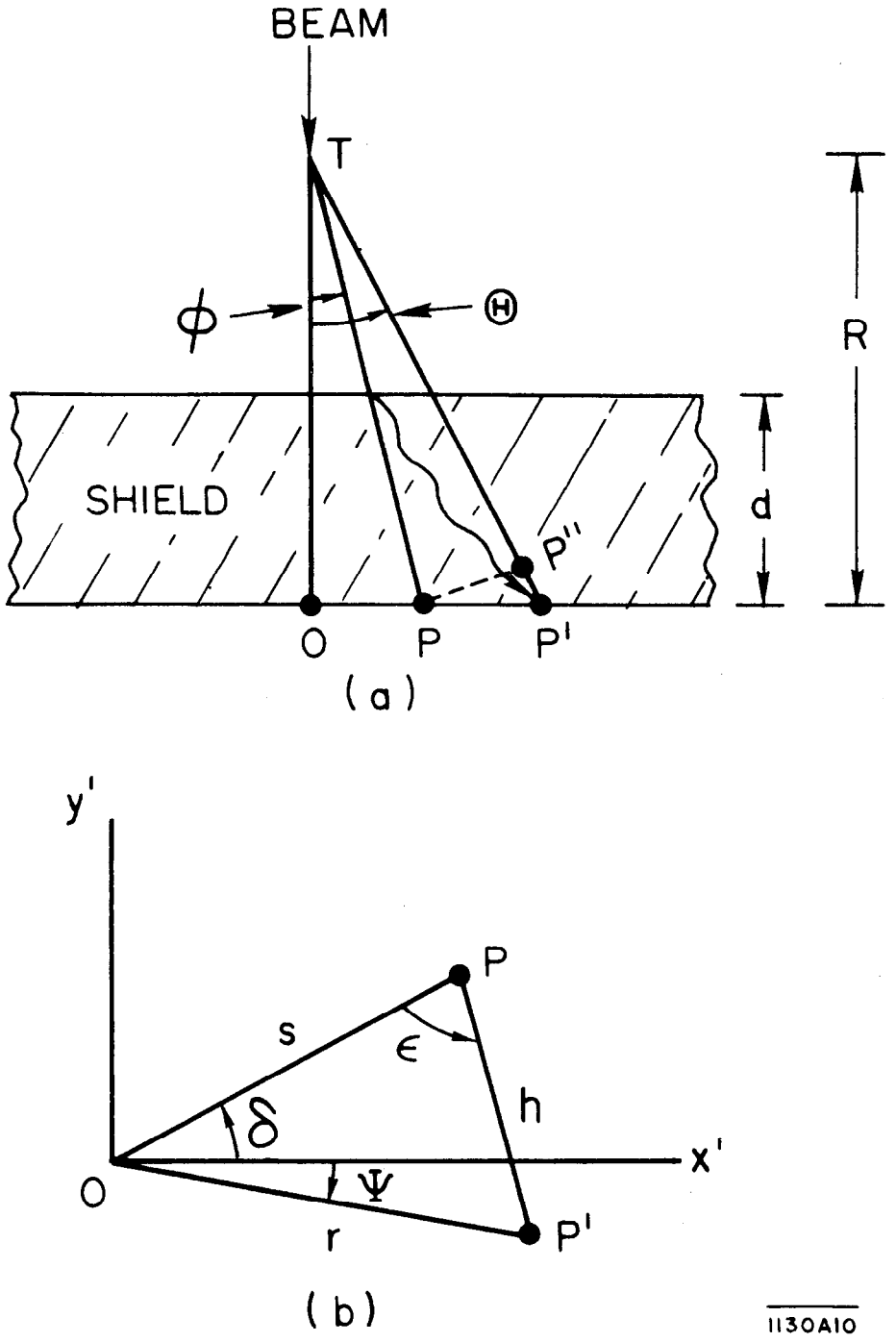
BEAM
T
ϕ
Θ
R
SHIELD
d
P''
O
P
P'
(a)
y'
P
s
ϵ
h
δ
x'
O
Ψ
r
P'
(b)
1130A10

Fig. 8

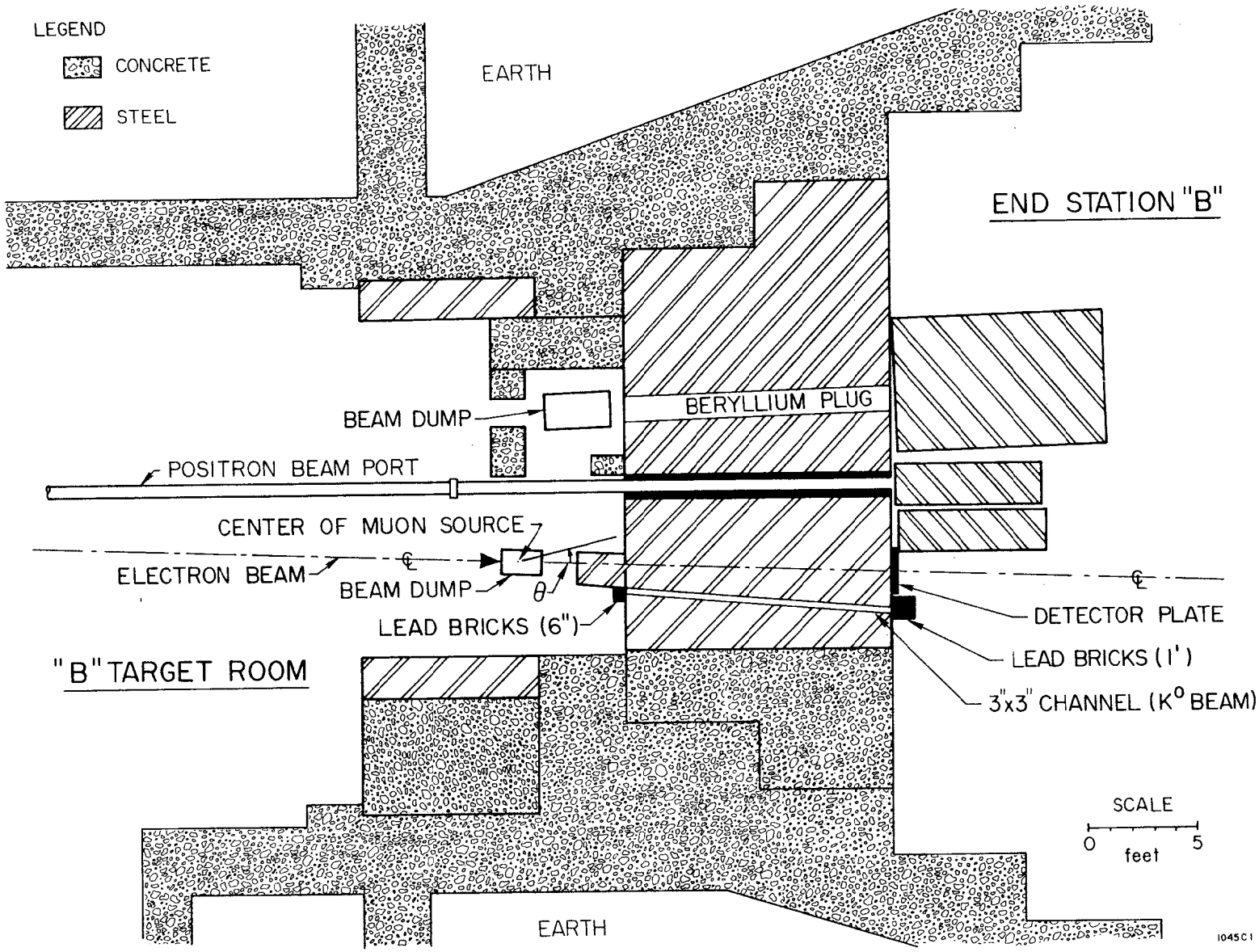
LEGEND
CONCRETE
STEEL
EARTH
END STATION "B"
BERYLLIUM PLUG
BEAM DUMP
POSITRON BEAM PORT
CENTER OF MUON SOURCE
ELECTRON BEAM
BEAM DUMP
θ
LEAD BRICKS (6")
DETECTOR PLATE
LEAD BRICKS (1')
3"x3" CHANNEL (K° BEAM)
"B" TARGET ROOM
SCALE
0
5
feet
EARTH
1045C1

Fig. 9

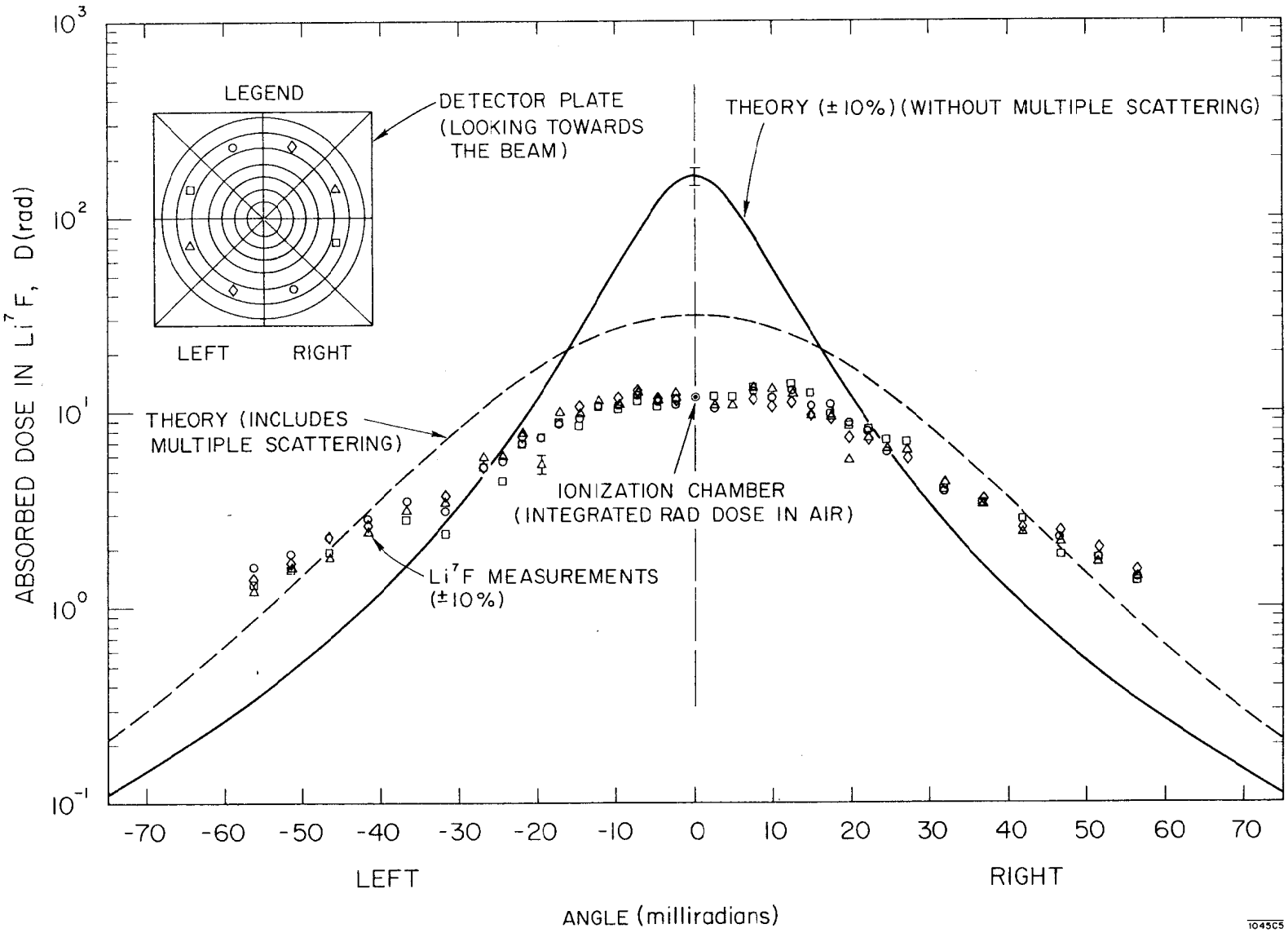
LEGEND
LEFT
RIGHT
DETECTOR PLATE
(LOOKING TOWARDS
THE BEAM)
THEORY (± 10%) (WITHOUT MULTIPLE SCATTERING)
THEORY (INCLUDES
MULTIPLE SCATTERING)
IONIZATION CHAMBER
(INTEGRATED RAD DOSE IN AIR)
Li7F MEASUREMENTS
(±10%)
ABSORBED DOSE IN Li7F, D(rad)
10^3
10^2
10^1
10^0
10^-1
-70
-60
-50
-40
-30
-20
-10
0
10
20
30
40
50
60
70
LEFT
RIGHT
ANGLE (milliradians)
1045C5

Fig. 10